MEASUREMENT OF DIESEL PARTICULATE EMISSIONS BY UV LIDAR REMOTE SENSING IN DENVER, CO, FEBRUARY 21-22, 2001

CRC Project E-56-1

August 2002

Prepared for:
Coordinating Research Council, Inc.
3650 Mansell Road, Suite 140
Alphareta, Georgia 30022

Prepared by:
Robert Keislar, Peter Barber, Hampden Kuhns, Claudio Mazzoleni,
Hans Moosmüller, Norm Robinson, and John Watson
Desert Research Institute
2215 Raggio Parkway
Reno, NV 89512-1095

ABSTRACT

On February 21-22, 2001 during the CRC Project E-56 field demonstration in Denver, CO, DRI obtained vehicle exhaust plume data using a field prototype of a LIDAR-based remote sensing system to measure particulate matter (PM) and a commercial remote sensor, the RSD3000 manufactured by Environmental Systems Products, Inc., to measure gaseous pollutants. In this report the theory and design of the LIDAR PM system is emphasized.

Measurements were made for three test vehicles, an Isuzu, a Ford van and a Ford pickup. The LIDAR PM measurements for both parking lot and freeway onramp conditions were highest for the Isuzu. Furthermore, PM measurements for the Ford pickup were higher for the Series 1 configuration than for the Series 2 configuration.

The LIDAR particulate matter system continues to be improved. As configured for this field test, uncertainty in the measurements occurs when the PM and CO_2 beams detect different portions of the exhaust plume. This problem has since been solved by developing a CO_2 channel (separate from that of the RSD3000) that is collinear with the LIDAR beam. A second limitation is that the sensitivity is not great enough. That is, while the system does an adequate job of detecting the particulates from high-polluting vehicles, it cannot detect the PM for low emitting vehicles. A solution for this problem is currently being pursued.

ACKNOWLEDGEMENT

We gratefully acknowledge the support of the Coordinating Research Council, Inc. for sponsoring this field demonstration. We also thank the other participating organizations, the Colorado Department of Public Health and the Environment and the Fuel Efficiency Automobile Test (FEAT) Group at Denver University. In particular, we thank Don Stedman of Denver University for his hospitality and technical input prior to and during this field demonstration and Gary Bishop of Denver University for providing the derivation of the fuel-based emissions factor that is included in the Appendix of this report.

TABLE OF CONTENTS

1. Introduction 1
1.1 Background 1
1.2 Objectives 1
1.3 Overview 1
2. Remote Sensing System 1
2.1 LIDAR-Based Remote Sensing of Vehicle Particulate Emissions 2
2.1.1 Theory 2
2.1.2 Light Scattering and Extinction Calculations 8
2.1.3 Laboratory Calibration 10
2.1.4 Field Measurements 11
2.1.5 Mass Density Calculation 11
2.1.6 Instrumentation 14
2.2 RSD3000 Gaseous Remote Sensing System 19
3. Experimental Setup 20
4. Experimental Results And Summary 23
4.1 Fuel Based Emissions Factor Calculation 23
4.2 Measurement Results 24
5. References 28

1. INTRODUCTION

1.1 Background

Remote sensing of vehicle exhaust is an economical way to determine on-road emissions for thousands of vehicles per day (Stedman and Bishop 1990). Remote sensing measurement of gaseous pollutants in vehicle emissions is well established. For example, the Fuel Efficiency Automobile Test (FEAT) system uses absorption measurements in the infrared and ultraviolet spectral regions to determine column concentrations of carbon monoxide (CO), carbon dioxide (CO_2), hydrocarbons (HC), and nitric oxide (NO) in the exhaust plume of individual passing vehicles. Emission factors (per fuel consumption) can be derived by taking the ratio of CO, HC, and NO to CO_2.

In addition to gaseous pollutants, recent results (Lawson and Smith, 1998) have increased interest in developing a remote sensing method for measuring on-road particulate matter emissions from gasoline-powered and diesel-powered vehicles. Measurement of particulate matter in exhaust has been made on a dynamometer with direct collection onto filters (Sagebiel et al. 1997; Cadle et al. 1997). On-road measurements of light absorbing particle emissions have been made both with an aethalometer (Hansen and Rosen 1990) and with the University of Denver (DU) opacity method (Morris et al. 1998). Aethalometer measurements cannot assign emissions to single vehicles in dense traffic, and the DU method is relatively insensitive.

DRI has developed a prototype LIDAR-based remote sensing system for the measurement of on-road particulate matter emissions. With suitable assumptions regarding size distribution and particle composition, the LIDAR backscatter signal can be used to estimate particle mass emissions. With an approximate collinear measurement of CO2 across the plume, the particulate mass emission factor (per fuel consumption) can be obtained.

1.2 Objectives

The primary objectives of this project are to demonstrate the LIDAR backscatter method for the measurement of PM emissions and to compare the LIDAR backscatter method to the conventional opacity method in a controlled setting. Conventional remote sensing of gaseous vehicle emissions complement the PM measurements.

1.3 Overview

Section 2 of this report describes the remote sensing system theory and instrumentation. Section 3 describes the two days of testing, the first in the Denver University parking lot and the second at the northbound on-ramp of I-25 from northbound University Blvd. Section 4 summarizes the data processing and presents results.

2. REMOTE SENSING SYSTEM

The DRI Vehicle Emissions Remote Sensing System is comprised of two main systems: a prototype of the LIDAR-based PM measurement hardware, referred to herein as LORAX (Lidar On-Road Aerosol eXperiment), and a commercial remote sensor of gaseous pollutants, the RSD3000, manufactured by Environmental Systems Products, Inc (ESPi). The theory and

instrumentation of these two systems are described in the following subparagraphs, with particular emphasis on the LIDAR system.

2.1 LIDAR-Based Remote Sensing of Vehicle Particulate Emissions

2.1.1 Theory

The light detection and ranging system (LIDAR) developed by the Desert Research Institute is designed to measure particle mass (PM) in a column defined by the laser beam through an exhaust plume. Simultaneously, an infrared source is used to detect the CO_2 in a similar column through the exhaust plume. The ratio of PM to CO_2 gives a relative measure of the pollution being generated by the vehicle in grams of PM per unit of fuel carbon consumed. This report will focus on the LIDAR measurement of PM.

When light illuminates a small particle such as a pollution particle in an exhaust plume, the light is both scattered in all directions and absorbed by the particle. For a particular incident light beam, the nature of the scattering and absorption interaction is determined by the physical characteristics of the individual particles – their size, shape, and material characteristics - as well as by the size and shape distribution of the suspension of particles. If the characteristics of the incident light are known, specifically its direction of propagation, polarization, wavelength, and intensity, then this knowledge, coupled with the nature of the scattered light and a laboratory calibration, can be used to determine some features of particles in an exhaust plume.

The light scattered by a particle or suspension of particles back in the direction of the incident light is known to be particularly sensitive to the physical characteristics of the particle. Analysis of this "backscattered" light to determine particle characteristics is analogous to what is done with radar, whereby microwave radiation is "bounced" back from an unknown airborne target to determine its identity. The sensitivity of detection of the backscattered light can be maximized by choosing a light source at a wavelength that is comparable to the size of the particles being measured. Soot in vehicle exhaust generally falls in the size range of 0.1 to 1.0 μm.

In the remote sensing system utilized here, a narrow pulse (nominally 1 ns in duration) at an ultraviolet wavelength of 0.266 μm leaves the transmitting laser at one side of the road and is partially reflected back toward the transmitter by particles in the exhaust plume. The received signal is the output of a photo-multiplier tube (a voltage) vs time. The dimensions of the typical roadside configuration are such that the 1 ns pulse (traveling at the speed of light) interacts with the exhaust plume and the beam termination and is returned in less than 100 ns. For the given pulse repetition frequency of 6.8 KHz, a pulse is transmitted approximately every 150 μs, ensuring that only a single 1 ns transmitted pulse interacts with the exhaust plume at a time. The roadside remote sensing configuration is shown in Fig. 1.

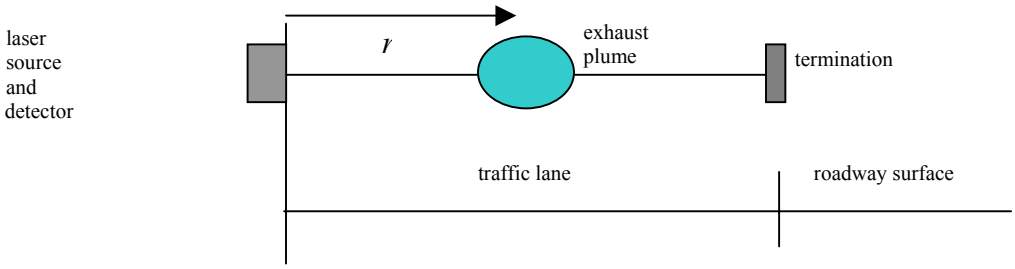

Fig. 1. LIDAR configuration. The range variable is *r*.

The single-particle differential scattering cross section in the backscatter direction and the single-particle extinction cross section provide the particle information that is required to predict the received power that can be measured by a LIDAR system.

The basic operation of the system is defined by the LIDAR equation (Measures 1992),

$$P(r) = P_L O(r) \frac{c\tau}{2} \frac{A}{r^2} \sum_i [N_i(r)\sigma_{d,i}(r,\pi)] e^{-2\sum_i \int_o^r N_i(r')\sigma_{e,i}(r')dr'} \quad (1)$$

where

$P(r)$ = scattered laser power (Watts) received at the detector at a time corresponding to the leading edge of the laser pulse propagating to a range r, meters.

$O(r)$ = characterizes the overlap (zero to unity) of the receiving telescope field of view with the UV-laser illuminated particulate path.

P_L = average power (Watts) of the incident laser beam.

c = speed of light, 3 x 10^8 m/s.

τ = incident beam pulse width, s.

A = area of receiver telescope aperture, m^2.

$N_i(r)$ = number density of scatterer species i, #/m^3, at range r.

$\sigma_{d,i}(r,\pi)$ = differential scattering cross section of species i in the backscatter (π) direction, m^2/steradian, at range r.

$\sigma_{e,i}(r)$ = extinction cross section of species i, m^2, at range r.

i = an index denoting a particle that has a specific size, shape, and composition. Eq. (1) includes a summation over all of the different particles that may be present.

The term $N_i(r)\,\sigma_{d,i}(r,\pi)$ in (1) quantifies the backscattering from particles of species *i*. The term $N_i(r')\,\sigma_{e,i}(r')$ in the exponent quantifies the extinction from particles of species *i*, where the factor of 2 accounts for the roundtrip two-way extinction experienced by the LIDAR pulse. Therefore, the initial amplitude of the backscattered pulse diminishes at later times during the two-way attenuation of the pulse by the scattering and absorption (the sum is the extinction) of the intervening particles.

In general, three species *i* are of interest: (1) the PM in the exhaust plume of the vehicle being measured, (2) the background molecular gases in the atmosphere, and (3) the ambient PM. This latter quantity may include multiple components, such as the background PM from regional sources, PM from vehicles that immediately preceded the vehicle currently being measured, and dust particles raised from the road surface by vehicle motion and roadway tire contact. For purposes of the present analysis, species (2) and (3) will be incorporated in a single ambient term.

The form of the LIDAR equation in (1) incorporates a number of assumptions that simplify the analysis. However, none of these assumptions detract from our ability to use (1) to understand the factors that determine the received laser power. Two important assumptions are that the incident laser signal is a rectangular pulse (in time) and monochromatic (single wavelength) and the spatial distribution of PM in the exhaust plume is homogeneous.

The LIDAR equation will be analyzed by first considering the combined effect of the scattering from two species of particulates – PM in an exhaust plume and an ambient background consisting of only atmospheric molecular scattering. Once this situation is illustrated, then it is straightforward to incrementally add additional ambient terms, including background regional PM, PM from preceding vehicles, and dust.

For a homogeneous particulate distribution within the plume, the exponential term in (1) can be simplified, since $N(r')$ and $\sigma_e(r')$ are constant with *r*. For a system consisting of two species of particles, background molecular gases and PM in the exhaust plume, the term in the exponent in (1) becomes,

$$-2\{N_a\,\sigma_{e,a}\,r + N_{PM}\,\sigma_{e,PM}\,[r\text{-}r_o]\}, \qquad (2)$$

where the quantities with the subscript *a* are associated with molecular gases and variables with the subscript *PM* are associated with the exhaust plume. Then (1) becomes

$$P(r) = P_L O(r)\frac{c\tau}{2}\frac{A}{r^2}\sum_i [N_i\sigma_{d,i}(\pi)]e^{-2\{N_a\sigma_{e,a}r + N_{PM}\sigma_{e,PM}[r-r_o]\}}, \qquad (3)$$

where r_o is the range distance to the leading edge of the plume.

Here it is important to remember that $\sigma_{d,i}(\pi)$ and $\sigma_{e,PM}$ only have value within the plume and are zero when the range variable *r* is not within the plume.

It is useful to consider the special case when the quantity in (2) can be approximated as zero. This assumes that the extinction by both the ambient particles and the PM in the exhaust plume are negligible. The extinction by molecular gases (the first term) over the limited range of the system will be quite small. In the case of the exhaust plume (the second term), this term will be

small when the product $N_{PM}\sigma_{e,PM}$ is small, either because the particle density N_{PM} in the plume is low or the particles in the plume have low extinction coefficients, or the thickness of the plume is small, or some combination of all three factors. When the quantity in (2) is negligibly small, e^{o} = 1 in (3) and (3) becomes

$$P(r) = P_L O(r)\frac{c\tau}{2}\frac{A}{r^2}\sum_i [N_i(r)\sigma_{d,i}(\pi)]. \qquad (4)$$

Except for the $O(r)$ and $1/r^2$ terms, the term preceding the summation is a system constant that can be represented by C_o. Making this substitution and expanding the summation in (4) gives,

$$P(r) = \frac{C_o O(r)}{r^2}[N_a\sigma_{d,a}(\pi) + N_{PM}\sigma_{d,PM}(\pi)]. \qquad (5)$$

The first term in brackets, the backscatter from molecular gases, includes no range dependence – it exists across the entire range. The second term, as mentioned earlier, is zero outside the plume and has value only when the range variable r is within the plume. Both terms decrease as $1/r^2$ with range r.

Eq. (5) also describes the temporal behavior since $r = ct/2$. If the leading edge of the laser pulse leaves the source at time $t = 0$, then the scattered power is received at the detector as some later time $t = 2\ r/c$, where the factor of 2 accounts for the round trip transit time. Scattered power from the exhaust plume is only received when the pulse overlaps the plume. There are three distinct regions of overlap – when the pulse is entering the plume, when the pulse is entirely within the plume, and when the pulse is exiting the plume.

As an example, consider an arrangement where the total path length is 11 m with a 1 m thick exhaust plume located at the center. The first signal to arrive back at the receiver is from the leading edge of the incident pulse entering the exhaust plume at a distance of 5 m. This occurs when $t = (2)(5\text{ m})/3 \times 10^8$ m/s = 33.3 ns. Scattered power from the pulse interaction with the leading edge of the plume will continue to be received until the trailing edge of the pulse is at 5 m, which occurs 1 ns later, so the last signal from the leading edge of the exhaust plume arrives at 34.3 ns. The last signal from the exhaust plume arrives at the receiver when the trailing edge of the pulse is leaving the trailing edge of the plume at a distance of 6 m. The leading edge of the pulse is at 6 m when $t = (2)(6\text{ m})/3 \times 10^8 = 40$ ns. Signal will continue to be received until the trailing edge of the pulse is at 6 m, which occurs 1 ns later, so the last signal from the trailing edge of the exhaust plume arrives at 41 ns.

The reflected signal from the beam termination is received when $t = (2)(11\text{ m})/3 \times 10^8 = 73.3$ ns. The duration of the beam termination signal is 1 ns.

The received LIDAR power for the two-species system defined by (5), background molecular gases and exhaust PM, is qualitatively described, for this example, by Fig. 2.

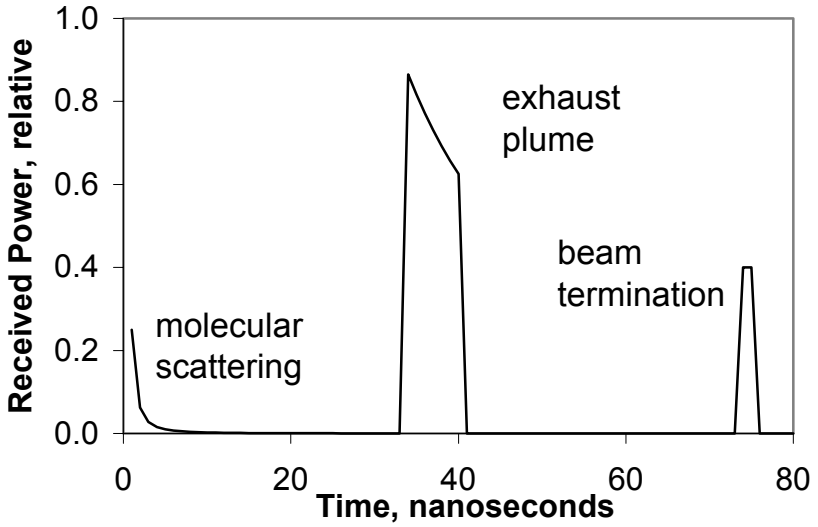

Fig. 2. LIDAR signal for a 1 ns pulse transmitted at $t = 0$.

Note that the received power from the exhaust plume increases between 33.3 and 34.3 ns as the incident 1 ns pulse enters the plume, decreases as $1/r^2$ as the pulse transits the plume, and then decreases between 40 and 41 ns as the incident 1 ns pulse exits the plume. The received power from the background molecular scattering is only observable at early times, when the transmitted pulse is close to the source. At later times the molecular scattering is significantly reduced by the $1/r^2$ term in (5). The returned power from the beam termination has been given an arbitrary amplitude for purposes of this example.

This has been a qualitative example. A quantitative simulation of the LIDAR process defined by (5) requires specific knowledge of the exhaust PM and its scattering and extinction characteristics.

For vehicle (gasoline and diesel) exhaust, it is necessary to determine the physical characteristics of the particles contained within the plumes, i.e., their size, shape and index of refraction (related to composition), so that the quantities $\sigma_d(\pi)$ and σ_e may be approximated or calculated, thereby enabling backscattering and extinction calculations (Barber and Hill 1990). This information requires some knowledge of the form in which elemental carbon and organic carbon are present in the particulate distributions – as separate particles, homogeneous spherical mixtures, agglomerations, or in layered configurations. In addition to the characteristics of individual particles, we need to know the particle size and shape distributions that may be expected for vehicle exhaust. A number of studies have considered the above factors.

2.1.1.1 Vehicle Exhaust Characteristics

Horvath (Horvath 1993) focuses on the properties of black carbon and its (exclusive) role in absorption in the atmosphere. He indicates that for atmospheric particles, only elemental carbon, the main constituent of black carbon, is highly absorbing. His Table I summarizes 15 refractive indices that have been used for elemental carbon. Real parts of the refractive index vary from 1.5

to 2.0 and imaginary parts vary from 0.1 to 1.0. He indicates that light-absorbing particles are only formed by combustion processes, where the majority are of anthropogenic origin. Incomplete oxidation of the carbon-containing fuel causes the formation of black carbon. Major sources of elemental carbon in the atmosphere are diesel motors and small furnaces, as well as biomass burning. For vehicles, black carbon emissions from pre-1992 diesel engines are about 100 times those of a hot-stabilized gasoline engine for an equivalent driving distance. A specific example for a particular pre-1992 diesel engine shows that the emitted particulates can contain both elemental and organic carbon, with the fraction of each varying from 10% to 90% depending upon the quality and the operating conditions of the engine.

Völger et al (Volger et al 1996) give a table of refractive indices of aerosol components at different wavelengths. Specifically, the refractive index of soot at wavelengths of 250 nm and 300 nm, is given as 1.62- i0.45 and 1.74-i0.47, respectively.

Kittleson (Kittleson 1998) indicates that particulate mass emissions from pre-1992 heavy duty diesel engines typically are 10-100 times higher than those from spark ignition engines. The structure of unaged diesel exhaust particles is shown in his Fig. 1 as agglomerated solid carbonaceous material, ash, and volatile organic and sulfur compounds. His Fig. 3 shows a typical engine exhaust size distribution, for both mass and number weighting. Most of the particle mass exists in the 0.1-0.3 μm diameter range. This is where the carbonaceous agglomerates and associated adsorbed materials reside. The nuclei mode typically consists of particles in the 0.005-0.05 μm diameter range. This mode usually consists of volatile organic and sulfur compounds that form during exhaust dilution and cooling, and may also contain solid carbon and metal compounds. His Figs. 10 and 11 show number-weighted size distributions for two specific diesel engines.

Martins et al (Martins et al 1998) use a layered-sphere configuration to model biomass burning particles. The model consists of a highly-absorbing black-carbon core surrounded by a much lower absorbing shell. They indicate that this low-absorbing shell is likely formed by gas-to-particle conversion and condensation of volatile compounds. At a wavelength of 0.55 μm, the refractive index of the black carbon is assumed to be 2.0-i1.0 and that of the low-absorbing shell is assumed to be $1.5 - i10^{-6}$.

Shi et al (Shi et al 2000) have determined the physical properties (size distribution, number, volume, mass concentrations, and density), chemical properties (organic and elemental carbon, PAH, sulfate, and nitrate), and morphology of particles of a particular diesel engine. They found wide variations in particle size distributions and number concentrations depending upon dilution conditions and humidity. They found that combustion particles are largely present in the form of clusters. Large particles were found to be clusters of small basic particles that ranged from 10 to 40 nm. Their measurements provide some confirmation that emitted particles consist of a nonvolatile core covered by a volatile liquid material.

Bessagnet and Roset (Bessagnet and Roset 2001) focus on the plume emitted by diesel vehicles. They indicate that recent studies have shown that particles exist as aggregrates of carbon spherules displaying linear to quasi-spherical structures. Fresh combustion particles, presumably elemental carbon spheres, each about 20-30 nm in diameter, are emitted together with sulfuric acid, water vapor and a number of other species, including volatile organic species, at vehicle exhaust pipes. These nucleate, condense and are absorbed on the carbonaceous particles. Their Fig. 1 is a schematic drawing that depicts the evolutionary processes that occur immediately at

the exit of the vehicle exhaust system. They indicate that emissions from vehicle exhaust occur under different meteorological conditions that can influence the composition of the plume. This pertains particularly to humidity. Furthermore, the makeup of the emission depends strongly upon vehicle type and operating conditions. One example shows that the mass fraction of dry aerosol emitted in the exhaust of a diesel vehicle is 15.76% elemental carbon and 83.65% organic carbon, with much smaller percentages of other components. The size distribution of particles has been simulated in the immediate area of the exhaust pipe. A nucleation burst occurs at the exit of the exhaust pipe and intense coagulation follows, such that in only a few meters a bimodal particle spectra with peaks at 5 and 60 nm occurs (their Fig. 3a).

The selection of particulate models to use in the mathematical simulation of the LIDAR interaction with vehicle exhaust involves a tradeoff. The particulate systems are so complex and variable that it is unlikely that exact particle models can be formulated. Furthermore, even if an exact model could be formulated, the ability of available electromagnetic scattering and absorption computer programs to obtain numerical results is restricted to a small class of particle configurations. In the end, the goal is to obtain numerical results that will indicate the semi-quantitative behavior of the real-world light scattering and absorption interactions. For purposes of the present LIDAR simulation, the above considerations and information contained in the literature indicate that the use of a layered sphere model may be the best compromise between reality and our ability to obtain numerical results.

Furthermore, for purposes of this simulation, we will use an index of refraction for elemental carbon of $1.5+i0.5$ and for organic carbon of $1.5+i0.0$. Presumably these two components can appear together in the same particle – the most commonly assumed configuration is a layer of organic carbon condensed upon an elemental carbon base particle.

The literature shows wide agreement that the number distribution of the particles in vehicle exhaust is a log-normal size distribution. The rough diameter of pollution particles in vehicle exhaust peaks around the 0.1 to 0.2 μm range. The paper by Bessagnet and Roset (Bessagnet and Roset 2001) for diesel engines probably is the most useful in defining number distributions for different cases.

2.1.2 Light Scattering and Extinction Calculations

It is clear from the previous discussion that the quantities of interest are the particle differential scattering cross section in the backscatter direction, $\sigma_d(\pi)$, and the particle extinction cross section, σ_e. These calculations have been made for particle diameters from 0.01μm to 10μm, encompassing the expected size range of vehicle exhaust particles. Results have been obtained for solid spheres (Barber and Hill 1990) with an index of refraction characteristic of organic carbon as well as for two-layer spheres (Toon and Ackermann 1981) consisting of an elemental carbon core and an organic carbon shell. The calculated quantities, $\sigma_d(\pi)$ and σ_e, have been normalized by particle volume. Calculations have been made for a wavelength of 0.266 μm, the ultraviolet wavelength of the LIDAR system.

Figure 3 shows the results of a calculation of $\sigma_d(\pi)$ and σ_e for a homogeneous spherical particle with an index of refraction of $m = 1.5 + i0.0$, representing a sphere of solid organic carbon. This particle is nonabsorbing (the imaginary part of the index of refraction is 0.0), so the extinction cross section σ_e is equal to the scattering cross section and, like the backscatter cross section $\sigma_d(\pi)$, exhibits a straight-line log-log behavior in the range 0.01 to 0.1 μm, indicative of the scattering behavior of particles that are small relative to a wavelength.

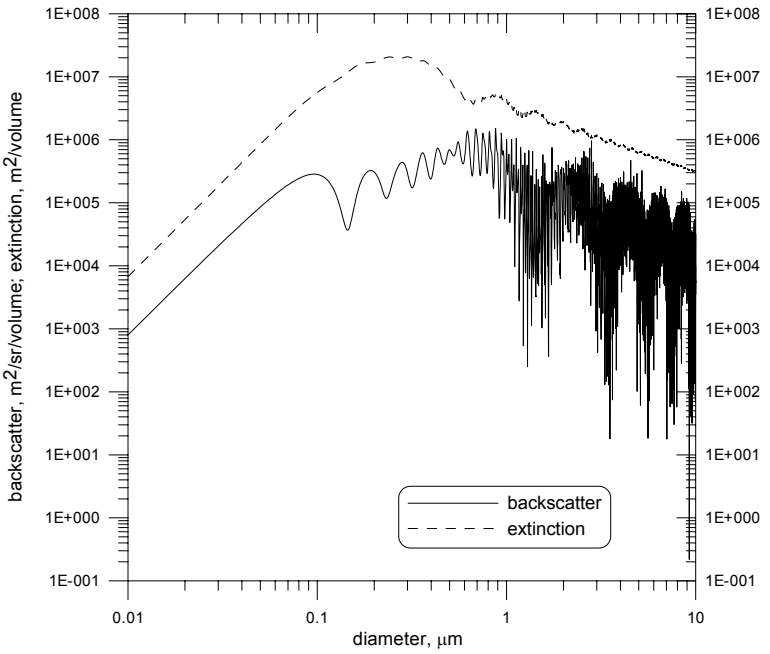

Fig. 3. Backscatter and extinction (normalized by particle volume) for a homogeneous spherical particle with an index of refraction of $m = 1.5 + i0.0$ at $\lambda = 0.266$ μm.

Figure 4 shows the result of a calculation for a layered spherical model consisting of an elemental carbon core surrounded by an organic carbon shell.

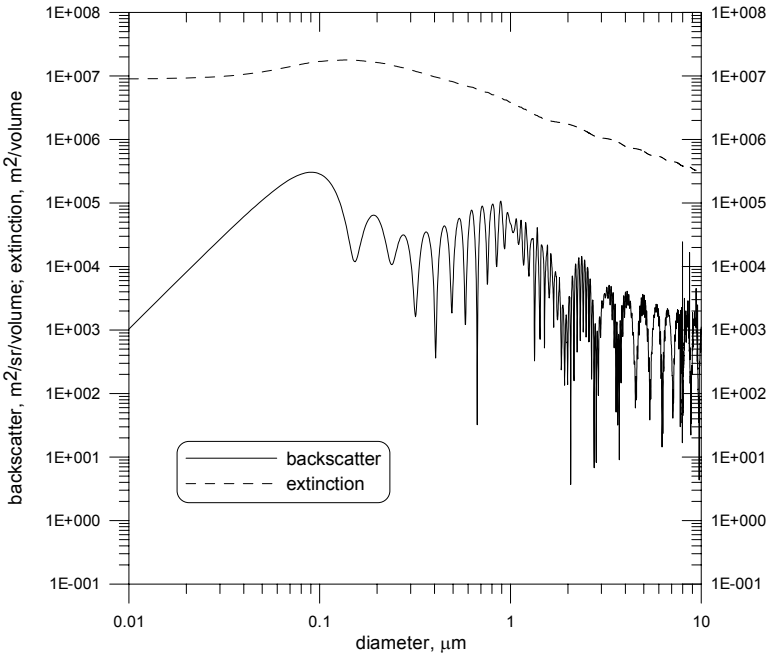

Fig. 4. Backscatter and extinction (normalized by particle volume) for a layered spherical particle with an index of refraction of $m_{core} = 1.5 + i0.5$ and $m_{\text{shell}} = 1.5 + i0.0$ at $\lambda = 0.266$ μm. Fractional core volume is 0.5.

2.1.3 Laboratory Calibration

The LIDAR return in an exhaust plume remote sensing application when the path extinction is assumed to be negligible is given by (5), where N and $\sigma_d(\pi)$ are generally functions of the range variable r, i.e., the particulate matter in the path changes in both number density and particle characteristics along the range.

In general, the ambient term includes the scattering from atmospheric molecules as well as the scattering from background particles, such as dust, particulate matter that may exist in the atmosphere on a regional basis, as well as lingering PM from a previous vehicle that may have transited the LIDAR remote sensing system. Two LIDAR measurements are made in the field, a pre-vehicle measurement and a post-vehicle measurement. We assume that the ambient term measured in the pre-vehicle measurement accurately describes the background when the post-vehicle measurement of vehicle exhaust is measured. Therefore, we subtract the ambient background from the vehicle exhaust measurement and obtain the scattered power from the particulates in the exhaust plume as

$$P(r) = \frac{C_o O(r)}{r^2}[N_{PM}\sigma_{d,PM}(\pi)]. \qquad (6)$$

Before field measurements are made, laboratory calibration of the system is necessary. This calibration includes a range correction to compensate for the nonuniform overlap of the receiving telescope field of view with the UV-laser illuminated particulate path and also to take out the $1/r^2$ dependence of the LIDAR returned signal. For purposes of the LIDAR measurement then, the general form of (6) is

$$P(r)\frac{r^2}{C_o O(r)} = N\sigma_d(\pi), \qquad (7)$$

where the units are 1/(m-sr). This signal is registered as a voltage (mV) at the terminals of the detecting photo multiplier tube (PMT) that converts the LIDAR optical signal to a voltage.

The range along the path can alternatively be described in terms of distance or time. For this application, the range correction is applied in the time domain at 0.25 ns intervals. In the laboratory we separately measure HEPA-filtered air and CO_2 with the LIDAR system. For both of these gases, the right hand side of (7) is known[1]. The value for the normal atmosphere at sea level under standard conditions of temperature (0 ˚C) and pressure (1013mb) and a wavelength of 266 nm is 2.55×10^{-5} 1/(m-sr). This is sometimes referred to as 1 Rayleigh unit to signify that the scattered return from molecules in the standard atmosphere is calculated using the Rayleigh approximation in scattering theory. The scattering return for CO_2 for the same conditions is 2.96 Rayleigh units.

In the laboratory measurements of HEPA-filtered air and CO_2, we know that the scattering should be uniformly constant across all range gates. The process of range correction is to make a laboratory measurement of the LIDAR received signal (in mV) at each range gate and then develop a procedure so that later field measurements can be related back to the absolute measurements that were made in the laboratory. We take measurements for both HEPA-filtered air and CO_2 in the laboratory because the signal correction at each range gate is assumed to be linear, (i.e., following the equation $y = mx + b$), and we need to determine the slope m and y-intercept b at each range gate – two measurements will give us the two unknowns.

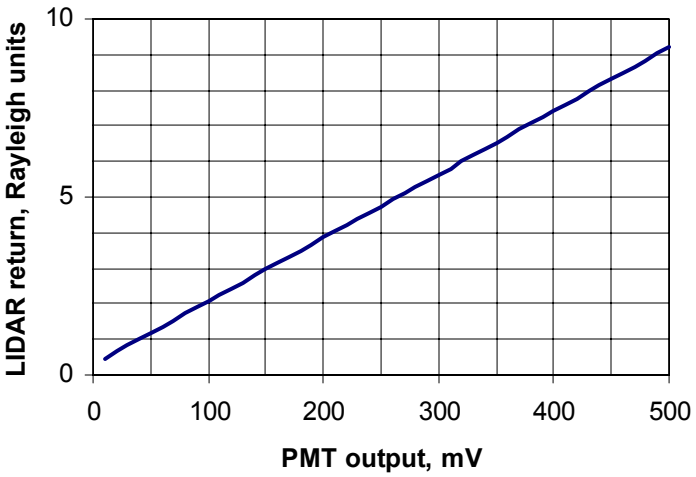

Fig. 5. LIDAR Calibration Curve

The procedure can be illustrated by reference to Fig. 5, the laboratory-derived calibration curve for a particular range gate. Assume that for this range gate, a laboratory measurement for HEPA-filtered air has produced a PMT output of 40 mV. This is known to correspond to a LIDAR scattering amplitude of 1 Rayleigh unit (2.55×10^{-5} 1/(m-sr)). A similar measurement for CO_2 has produced a PMT output of 150 mV and this is known to correspond to a LIDAR scattering amplitude of 2.96 Rayleigh units. Then the linear calibration curve can be drawn. A later field measurement of the PMT output for the LIDAR return from an exhaust plume can then be related back to the laboratory calibration. For example, a field measurement of 376 mV from an exhaust plume corresponds to a LIDAR return of 7 Rayleigh units or $7 \times 2.55 \times 10^{-5}$ 1/(m-sr) = 0.178×10^{-3} 1/(m-sr).

2.1.4 Field Measurements

The laboratory calibration provides us with a procedure for converting the field measurements of PMT voltage to absolute LIDAR return in terms of Rayleigh units. Specifically, with reference to (7), we can write the unknown PM scattering as,

$$N_{PM}\bar{\sigma}_{d,PM}(\pi) = R_{PM} N_{cal}\sigma_{cal}(\pi), \qquad (8)$$

where $N_{cal}\,\sigma_{cal}(\pi)$ is 2.55×10^{-5} 1/(m-sr) and R_{PM} is the LIDAR return from the exhaust plume in dimensionless Rayleigh units as determined from a field measurement (mV) and Fig. 5. Note that we use the mean differential scattering cross section in the backscatter direction, $\bar{\sigma}_{d,PM}(\pi)$. The quantities on the right hand side of (8) are all known from the laboratory calibration and a field measurement.

2.1.5 Mass Density Calculation

We now have a prescription, with some assumptions, for finding the mass density of particulate matter in the exhaust plume. N_{PM} in (8) is the number of particles per unit volume, #/m^3. If this quantity can be determined and if the mean mass of the exhaust particles is $\bar{m}$ kg, then the PM mass density M_{PM} is

$$M_{PM} = N_{PM}\ \overline{m}\ , \text{kg/m}^3. \tag{9}$$

To obtain N_{PM} it is necessary to determine the quantity $\overline{\sigma}_{d,PM}(\pi)$ on the left hand side of (8), the differential scattering cross section in the backscatter direction. We can calculate $\overline{\sigma}_{d,PM}(\pi)$ for a size distribution of solid spheres of organic carbon to represent the exhaust particles from spark-ignition vehicles and for a size distribution of layered spheres consisting of a core of elemental carbon surrounded by a shell of organic carbon to represent the exhaust particles from diesel-powered vehicles.

We make the further assumption that the particles in the exhaust can be represented by a normalized (to N) log-normal distribution (Seinfeld and Pandis 1998) $n_N(D)$,

$$n_N(D) = \frac{1}{(2\pi)^{1/2} D \ln\sigma_g} \exp[-\frac{(\ln D - \ln \overline{D}_g)^2}{2\ln^2 \sigma_g}], \tag{10}$$

where D is the particle diameter and the log-normal distribution is defined by the particle median diameter $\overline{D}_g$ and the geometric standard deviation σ_g. For our purposes it is more convenient to define the particle mass median diameter $\overline{D}_{gm}$ than $\overline{D}_g$, but these two quantities are related (Seinfeld and Pandis 1998) as

$$\ln \overline{D}_g = \ln \overline{D}_{gm} - 3\ln^2 \sigma_g, \tag{11}$$

so

$$\overline{D}_g = \exp(\ln \overline{D}_{gm} - 3\ln^2 \sigma_g). \tag{12}$$

Representative values for $\overline{D}_{gm}$ and σ_g can be found in the literature for spark and diesel exhaust plumes.

Then we can calculate the mean differential scattering cross section in the backscatter direction for defined particulate systems as

$$\overline{\sigma}_{d,PM}(\pi) = \frac{\int_o^\infty \sigma_{d,PM}(\pi, D) n_N(D) dD}{\int_o^\infty n_N(D) dD}\ , \tag{13}$$

where $\sigma_{d,PM}(\pi, D)$ is the differential scattering cross section in the backscatter direction for a particle of diameter D.

The mean mass is given by,

$$\overline{m} = \frac{\int_o^\infty m(D) n_N(D) dD}{\int_o^\infty n_N(D) dD}, \tag{14}$$

where $m(D)$ is the mass of a particle of diameter D.

The process of obtaining the mass density M_{PM} can then be summarized:

1. From a remote sensing field measurement for a particular vehicle, obtain the exhaust plume PMT backscatter signal in mV.

2. Convert the PMT mV signal to Rayleigh units R_{PM} from the calibration curve represented by Fig. 5.
3. Calculate $\overline{\sigma}_{d,PM}(\pi)$ and $\overline{m}$ from (13) and (14), respectively, for a defined particulate distribution, for a spark-ignition or diesel vehicle, as applicable.
4. Obtain N_{PM} from (8) using $\overline{\sigma}_{d,PM}(\pi)$ and then solve (9) for M_{PM}, using $\overline{m}$.

The final form for M_{PM} is

$$M_{PM} = R_{PM} N_{cal} \sigma_{cal}(\pi) \frac{\int_o^\infty m(D) n_N(D) dD}{\int_o^\infty \sigma_{d,PM}(\pi, D) n_N(D) dD} \text{ kg/m}^3. \quad (15)$$

We evaluate the two integrals in (15) using a numerical technique, then take the ratio as indicated. Multiplying by $N_{cal}\,\sigma_{cal}(\pi)$ then gives the constant that relates mass density M_{PM} to Rayleigh units R_{PM}. The constant, which can be denoted as C_{PM}, can be written explicitly as,

$$C_{PM} = N_{cal} \sigma_{cal}(\pi) \frac{\int_o^\infty m(D) n_N(D) dD}{\int_o^\infty \sigma_{d,PM}(\pi, D) n_N(D) dD} \text{ kg/m}^3. \quad (16)$$

Before giving calculated results for C_{PM}, it is important to summarize the assumptions that have been made.

$N_{cal}\,\sigma_{cal}(\pi)$ represents the backscattering by the calibration gases in the laboratory. One value from the literature at standard temperature and pressure for air is 2.55×10^{-5} 1/(m-sr). New more precise measurements could provide a more accurate value for this constant. Furthermore, a recalibration that takes into account nonstandard temperature and pressure in the laboratory would result in a small change to this constant. The calibration curve represented by Fig. 5 assumes that the backscattering by CO_2 is 2.96 greater than that for air. Finally, the calibration curve in Fig. 5 is assumed to be linear and was obtained by taking two measurements, one for air and one for CO_2. Measurements for other calibration gases, or for one or both of these gases at other temperatures and/or pressures may show that the calibration curve deviates from a straight line. So there are at least four assumptions in the use of $N_{cal}\,\sigma_{cal}(\pi)$.

The evaluation of the integrals in (16) is based on the assumption that the PM particles are spherical in shape. Furthermore, the size distribution of the particles is assumed to be lognormal with a specific geometric standard deviation σ_g and mass median diameter $\overline{D}_{gm}$. The calculations here assume a value of 1.5 μm and 0.1 μm for these two quantities, respectively. We assume a particle mass density of 1250 kg/m^3. Selection of other values will result in a change in the calculated C_{PM}.

The calculation of $\sigma_{d,PM}(\pi, D)$ inside the integral in the denominator of (16) assumes that the PM of spark-ignition vehicles can be represented by a solid sphere of organic carbon with an index of refraction of $m = 1.5+i0.0$. Calculations for diesel vehicles assume that the PM can be represented by a layered sphere consisting of a spherical core of elemental carbon surrounded by a shell of organic carbon. The index of refraction of the elemental carbon core is assumed to be $m = 1.5+i0.5$. The volume fraction of the layered particles is assumed to be 50/50; i.e., the core and shell are of equal volume.

It is known that PM particles are not spherical, but rather consist of coagulated aggregates of possibly spherical building blocks. Nevertheless, the spherical particles assumed here do incorporate many of the known features of these particles, including the optically non-absorbing characteristics of organic carbon and the absorbing characteristics of elemental carbon. Furthermore, the size range of the particles is in the known size range of PM particles from spark-ignition and diesel vehicles.

There are also complex assumptions in replacing $\sigma_{d,PM}(\pi)$ with $\bar{\sigma}_{d,PM}(\pi)$ in (8) and in asserting the relationship in (9).

All of these assumptions enter into the calculation of C_{PM} in (16). Therefore, the conversion of Rayleigh units to PM mass density resulting from the use of this constant should be viewed as a best estimate at this time, given what is currently known. However, as new information is obtained and incorporated, some of the assumptions may be refined or eliminated. When this occurs, revised values of C_{PM} may be calculated and used to linearly scale previous field measurements.

Finally, we should note that the scale factor C_{PM} is calculated at each range gate, but is assumed to be the same for all range gates. The major assumption in this is that the size distribution of the PM particles is assumed to be the same at all range gates, although the number density of particles may be different at each range gate (as represented by the spatial variation of R_{PM}). The data reduction process obtains a value for R_{PM} at each range gate, then obtains an average value across all range gates for a particular vehicle. This linear process of data reduction does not invalidate the use of C_{PM} for converting the R_{PM} for each vehicle.

Given these assumptions we have calculated C_{PM} values of **0.16 mg/m^3** for spark-ignition vehicles and **0.18 mg/m^3** for diesel vehicles. These values can be used with a measurement of the PM backscatter in Rayleigh units and the exhaust CO_2 in kg/m^3 for each vehicle to obtain vehicle emission factors in units of mg of PM per kg of fuel burned. With suitable assumptions for vehicle average mileage, an emission factor can be obtained in units of mg of PM per mile.

2.1.6 Instrumentation

DRI has designed and built a LIDAR-based remote sensing device temporarily called the LIDAR On-Road Aerosol Experiment (LORAX). The device measures on-road particulate matter emissions from passing cars. With suitable assumptions regarding size distribution and particle composition, the lidar backscatter signal can be used to estimate particle mass emissions (as discussed in the preceding theory section). With an approximately collocated measurement of CO_2 across the plume, the particulate mass emission factor (per fuel consumption) can be obtained. In this study the column CO_2 measurements were made with the RSD3000 gaseous remote emissions remote sensing system. During analysis of the data, we learned that coincidence of the CO_2 measurement and the PM (LIDAR) measurement in the exhaust plume was not optimum. We have since developed a CO_2 system that is collinear with the LIDAR beam. This improved system is described here.

Figure 6 shows a functional schematic of the LORAX system. Three main subsystems comprise LORAX: 1) the transmitter, which includes an UV laser and guiding optics; 2) the receiver, which includes a refracting telescope and a photomultiplier tube; and 3) the data acquisition subsystem, which includes a 1.5 GHz, 8 Gigasample s-1 oscilloscope and an acquisition computer. In addition, there are three auxiliary subsystems: 1) an extinction measurement

subsystem, which includes a photodetector for a UV extinction measurement, 2) a triggering/safety subsystem, which includes optical gates and a mechanical shutter on the UV laser, and 3) an alignment system comprised of three guide lasers and appropriate targets.

Figure 7 shows a top view of the on-road setup, where the main LORAX (and the RSD3000) system can be placed on either the right or the left shoulder of a single lane of traffic. Passive components, (i.e., mirrors, absorbing plates, and retro-reflectors), are placed in the LORAX Beam Terminus on the opposite side of the road (and the Vertical Transfer Mirror for the RSD3000).

Figure 8 shows a layout of the LORAX instrument box, and Figure 9 shows the layout of the Beam Terminus, which sits across the traffic lane. The transmitter is a Nd:YAG laser (λ=1.034 μm), frequency-quadrupled to yield 266-nm ultraviolet light (Nanolase, Model 00211-150, Meyllan, France, distributed by JDS Uniphase Corp., Sunnyvale, CA). The laser has an average power of 1 milliwatt, pulse duration of approximately 1 ns, and a pulse repetition frequency of 6.8 kHz. A fused silica beam splitter directs a signal into a high-speed silicon detector (ThorLabs DET210, 0.8 mm2, Newton, NJ) for an oscilloscope trigger. A spatial filter helps remove fringes by focusing laser light onto a 75 μm aperature, then collimates the beam which also acts as a 2x beam-expander. Two bounce mirrors (Mirror 1 and the outgoing Mirror 2) direct the beam out across the lane of traffic where it scatters off particles in the beam path.

The receiver is a 2" refracting telescope. Backscattered light in the field of view of the telescope is focused onto a photomultiplier tube (PMT, Hamamatsu H6780-06, Tokyo, Japan). A solar-blind filter and a notch filter are added to reduce background light. The PMT current is dropped across a 50 Ω load into the oscilloscope (Infinium 54845A, Agilent Technologies, Sunnyvale, CA). With a laser pulse duration of one ns, range gates would be 15 cm wide. Actual range resolution through the electronics is approximately 25 cm. An acquisition computer receives the waveforms from the oscilloscope where a single shot is recorded approximately every 5 ms.

Like the RSD3000 system, LORAX is triggered by a beam unblock signal which follows a beam block signal after 0.2-0.4 second, indicative of a passing vehicle. The optical gates provide this triggering as well as a safety cut-off which closes the mechanical shutter. The average gasoline-powered vehicle is from 1.5-1.8 m wide, giving approximately 10-12 range gates across the back of a car. If the exhaust stream exits at the side of the car, more range gates of interest are possible. Scattering from the terminus plate indicates the end of each pulse after approximately 40-50 ns, depending on the distance from the transmitter to the terminus plate. With an approximate pulse repetition rate of 6.8 KHz, backscatter from 3400 pulses, with 20-25 range gates each, could be collected in the half-second following the passage of the car. However, with the present data acquisition system, only 100 waveforms are collected.

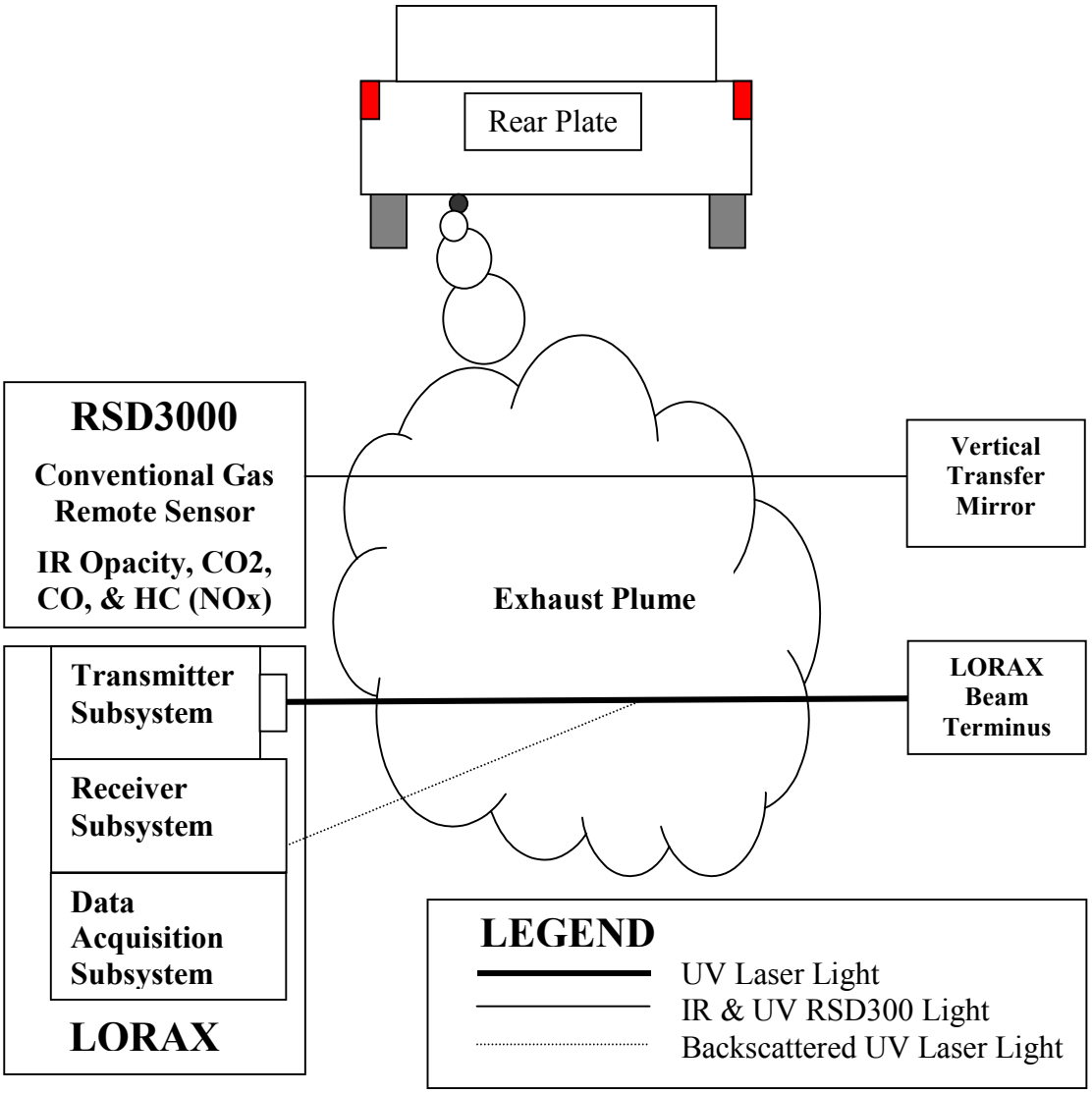

Figure 6. Functional schematic drawing of the LORAX System with the RSD3000 exhaust gas analyzer shown.

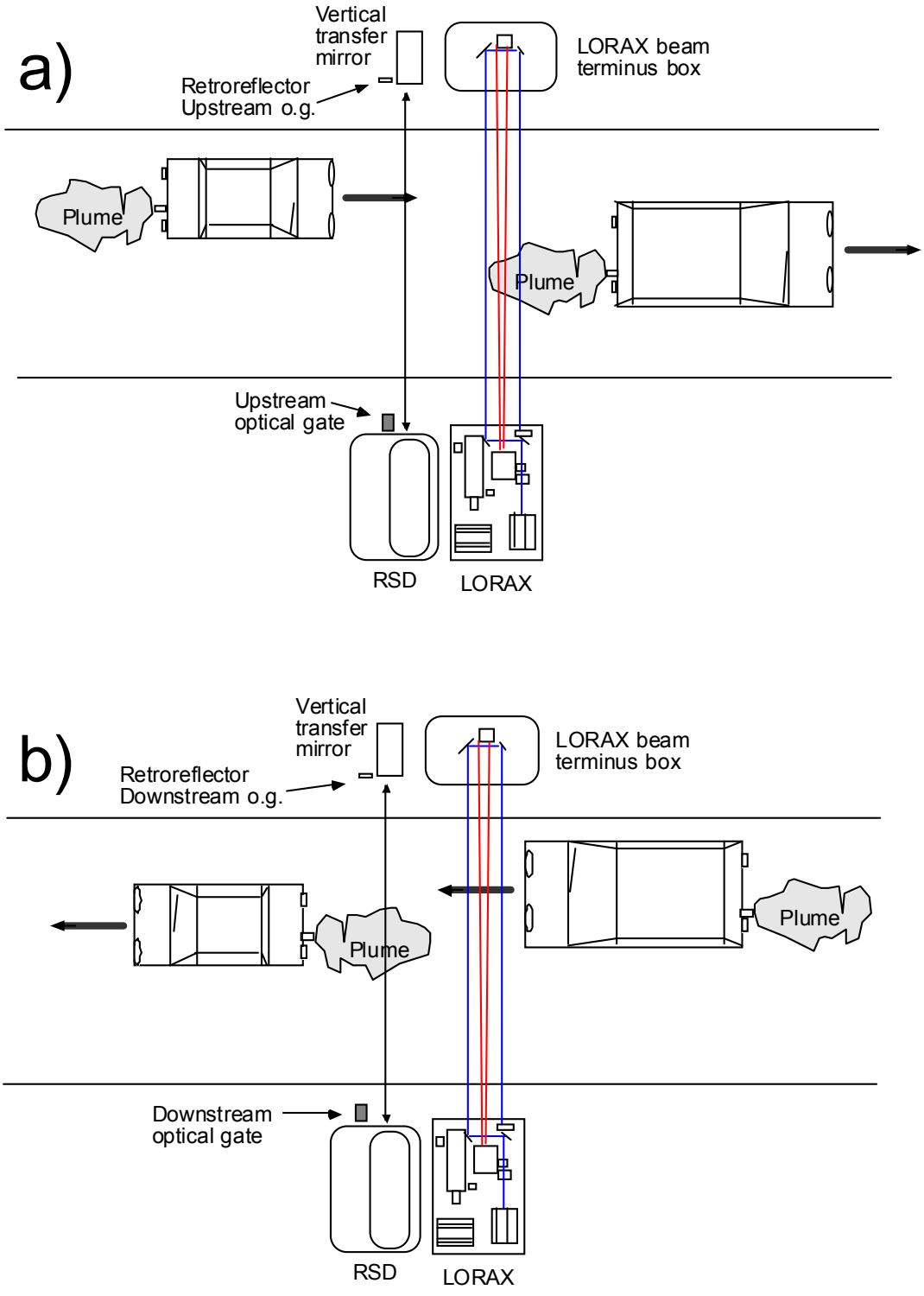

Figure 7. Top view of Lorax and RSD3000 setup on a) the right side of the traffic lane and b) the left side of the traffic lane. Processing is slightly different for the two scenarios, and the operator must enter either “Left” or “Right” in the initiation of the acquisition program.

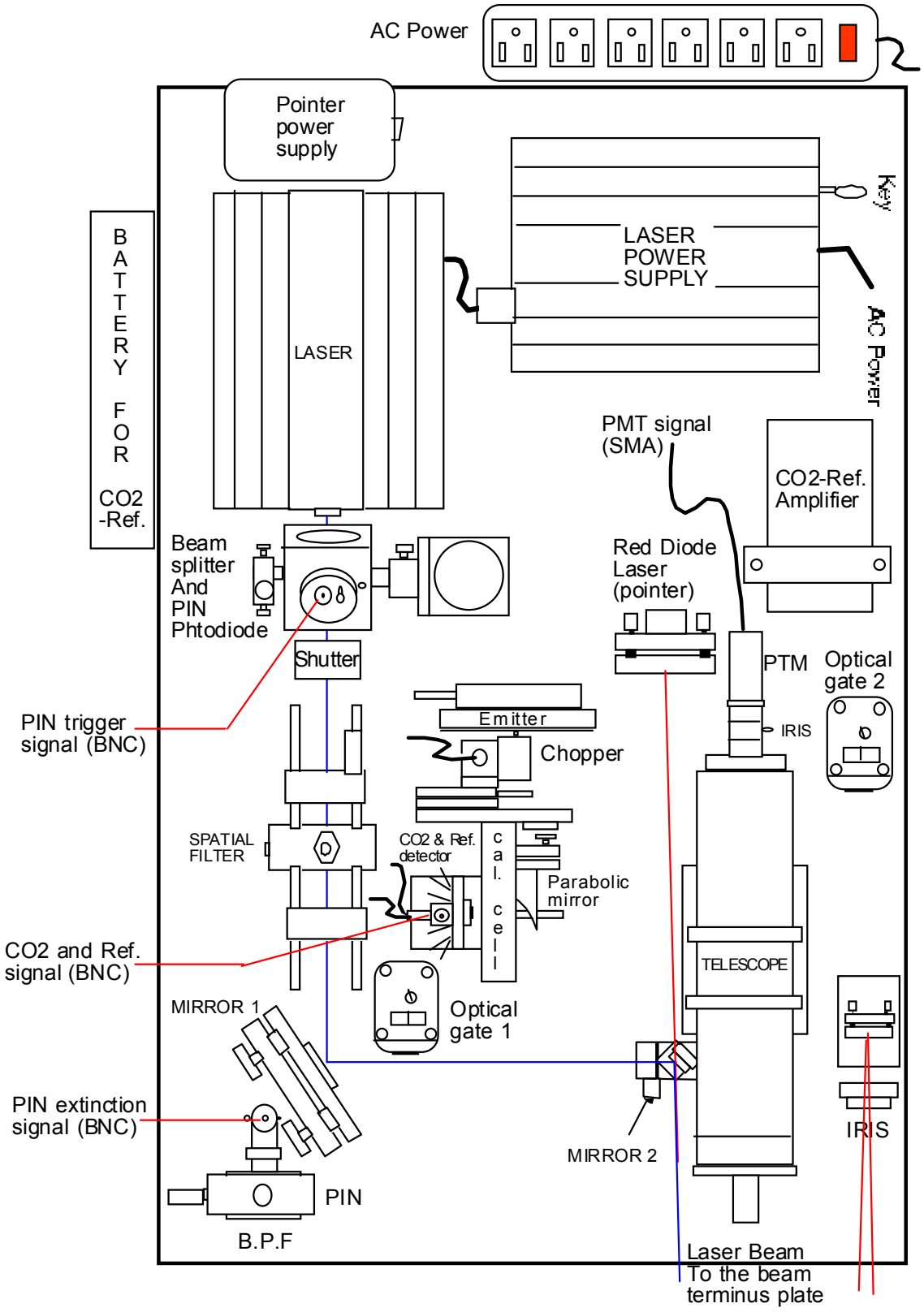

Figure 8. Layout of LORAX box.

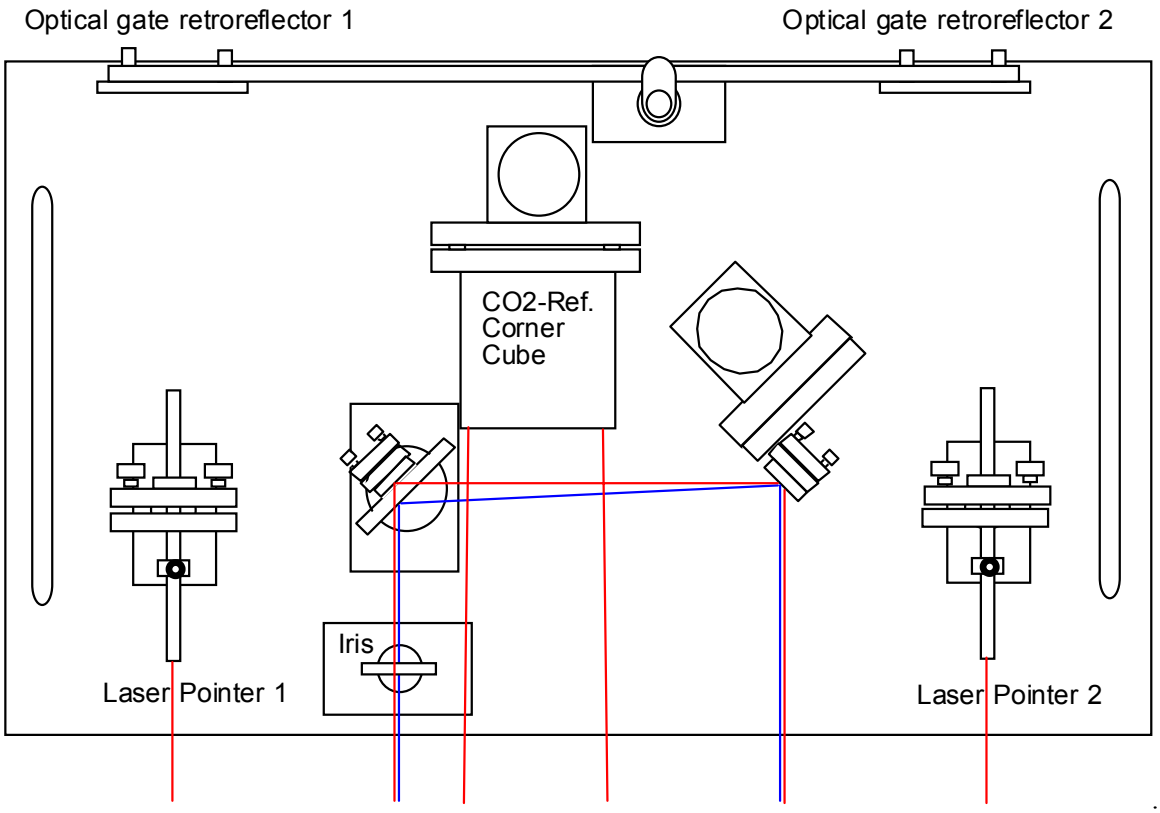

Figure 9. Layout of beam terminus.

Computer processing includes selecting the background LIDAR return and cataloging of sufficient time-stamps or other signals to link the LORAX data with the RSD3000 data.

The Beam Terminus box has two laser pointers for alignment, the beam terminus plate, which absorbs 99.99% of the laser energy, and three bounce mirrors to return the remaining laser light for the extinction measurement, and the third alignment laser in the Lorax box. Figure 9 also shows a corner cube used for the independent CO_2 channel, to be described in the final report. Retroreflectors for the optical gates are also housed in the Beam Terminus.

2.2 RSD3000 Gaseous Remote Sensing System

In 1987, the University of Denver developed an infra-red remote monitoring system for automobile carbon monoxide (CO) exhaust emissions. A hydrocarbon (HC) channel was soon added. Significant improvements in fuel economy result if rich-burning (high CO emissions) or misfiring (high HC emissions) vehicles are tuned to a more stoichiometric and more efficient air/fuel (A/F) ratio. Therefore, the University of Denver remote sensor was named Fuel Efficiency Automobile Test (FEAT). In 1991, Sun Electric was licensed to develop the FEAT patent into an off-the-shelf commercial product. In 1993, EnviroTest acquired Sun Electric, and the patent was licensed to Remote Sensing Technologies, Inc., a subsidiary of EnviroTest. Finally, in 1998, Environmental Systems Products, Inc. (ESPi) acquired EnviroTest. The current ESPi instrument, the RSD3000, measures CO, HC, carbon dioxide (CO_2), and nitric oxide (NO).

Automobile exhaust remote sensors, (e.g., the RSD3000), emulate the results one would obtain using a conventional non-dispersive infra-red exhaust gas analyzer, such as the NV94 Analyzer

used by emissions Test Stations to conduct State emissions tests. (Non-dispersive ultra-violet light is used for the NO channel.) An interference filter is placed in front of a detector to transmit light of a wavelength known to be absorbed by a molecule of interest. Reduction in the detector's voltage output is caused by absorption of light by the molecules of interest. Because the effective plume path length and amount of plume seen depends on turbulence and wind, one can only look at ratios of CO, HC, of NO to CO_2. These ratios are termed Q for CO/CO_2, Q' for HC/CO_2, and Q" for NO/CO_2, and are approximately constant for a given exhaust plume.

These ratios are useful parameters for describing the combustion system. With the aid of a fundamental knowledge of combustion chemistry, many parameters of the vehicle's operating characteristics can be determined including: the instantaneous air/fuel ratio, the %CO, %HC, or %NO which would be read by a tailpipe probe, and the grams CO, HC, or NO emitted per gallon of gasoline (Stedman and Bishop 1996). Since most new gasoline powered vehicles emit little CO or HC, they show a Q and Q' near zero, and often below the detection limit of the remote sensor. To observe a substantially larger Q, the engine must have a fuel-rich air/fuel ratio and the emission control system, if present, must not be fully operational. A high Q' can be associated with either fuel-rich or fuel-lean air/fuel ratios coupled with a missing or malfunctioning emission control system. A lean air/fuel ratio, while impairing driveability, produces very little CO in the engine. If the air/fuel ratio is lean enough to induce misfire, then a large amount of unburned fuel (HC) is present in the exhaust manifold. If a catalyst is absent or non-functional, then high HC can be observed in the exhaust without the presence of high CO. To the extent that the exhaust system of this misfiring vehicle contains some residual catalytic activity, the HC may be partially or totally converted to a CO/CO_2 mixture.

The height of the sensing beam is typically set at 20-30 cm above the road surface to observe exhaust plumes from light duty vehicles, provided the exhaust plume exits the vehicle within a few feet of the ground. The remote sensor is accompanied by a video system for vehicle identification information. The video camera is coupled directly into the data analysis computer so that the image of each passing vehicle is displayed on the video screen.

3. EXPERIMENTAL SETUP

A field demonstration was conducted in Denver, CO on February 21-22, 2001. DRI and Denver University participated in the demonstration near the Denver University campus. Figure 10 shows the test locations in relation to downtown Denver and the Denver University Campus.

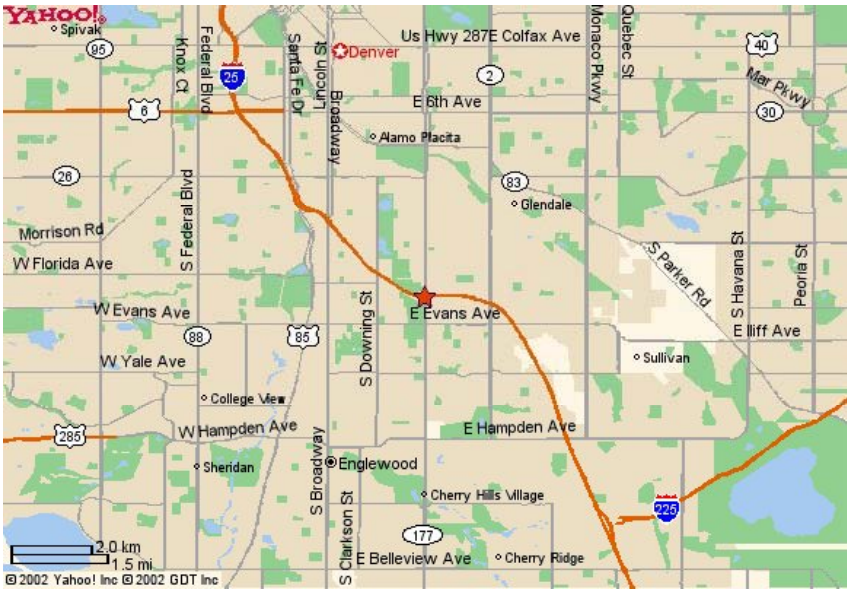

Figure 10. Site maps showing the University of Denver Campus (star in center of upper map) south-southeast of downtown Denver. An expanded map of the test area (lower map) showing the locations of the parking lot test on Day 1 (February 21, 2001) and the on-ramp test on Day 2 (February 22, 2001).

Three vehicles participated in the test:

1982 Isuzu Diesel Pickup (very "used" looking vehicle, some white to gray smoke emitted along with black smoke) - see Figure 11.

1986 Ford Club Wagon XLDiesel (full-sized van, some black smoke emitted) - see Figure 12.

2000 Ford F250 Pickup Diesel V8, Power Stroke in "clean" and "dirty" modes, (turbo, some black smoke emitted) - see Figure 13.

Figure 11. 1982 Isuzu Diesel Pickup

Figure 12. 1986 Ford Diesel Club Wagon

Figure 13. 2000 Ford Diesel F250 Pickup

The Ford F250 had an integrated circuit (chip) installed that would make the vehicle dirtier when activated. Both tests included the clean and dirty mode of the F250 as if they were separate vehicles. Therefore, there were four sets of passes in the parking lot. Each set consisted of five passes at each of three different speeds (10, 20, and 30 mph), making 15 passes per vehicle and a total of 60 passes (since the F250, with and without chip, counts as two vehicles). The parking lot had a 2.0% grade as the cars traveled approximately south-southeast.

The second day was an on-ramp test at Northbound I-25 from Northbound University Blvd. The ramp had a 2.2% grade at the sensors and comprised one 270^{o} turn of a symmetric cloverleaf interchange, around the other three turns of which the test vehicles passed to return to the northbound entrance ramp. On the on-ramp, 10 mph was deemed too dangerous (backed up traffic), and the vehicles were tested with five passes each at 20 and 30 mph. In addition, a series of accelerations (accels) were performed with the Isuzu (9 passes total) and the F250 (6 passes).

A Wagner Digital Smoke Meter, model 6500 was moved to the exhaust pipe of each vehicle during the tests for that vehicle. The vehicles had been previously dynamometer tested at constant velocity, with the same smoke meter, where the smoke meter was believed to be an adequate surrogate for total mass. Personnel from the Colorado Health Department selected the vehicles, performed the dynamometer testing, and performed the driving. The “accels” were not dynamometer tested, and the smoke meter surrogate for total mass is only considered valid for the constant-speed passes.

4. EXPERIMENTAL RESULTS AND SUMMARY

4.1 Fuel Based Emissions Factor Calculation

The RSD3000 and the LIDAR instrumentation report pollutant measurements in terms of a atmospheric mixing ratio (i.e. % or ppm) for gases or a mass concentration (i.e. ug/m^3) for particles. These values represent the concentration of a pollutant in the pure exhaust from the engine. For the purpose of emissions inventories, a fuel based emissions factor with units of g pollutant per kg fuel burned is preferred.

The fuel based emissions factors can be calculated from the pure exhaust concentrations by considering the stoichiometry of fuel combustion. The combustion reaction can be simplified to the following chemical equation assuming a H:C fuel ratio of 2:

$$CH_2 + m(0.21O_2 + 0.79N_2) \rightarrow aCO + bH_2O + c(C_3H_6 + invisible\ C_3H_6) + dCO_2 + eNO + \left(0.79m - \frac{e}{2}\right)N_2$$

Note the invisible C3H6 refers to the unseen exhaust hydrocarbons associated with remote sensing measurements of hydrocarbons using filtered infrared light. Using the assumptions and derivation shown in the Appendix (Bishop, personal communication 2002), the fuel based emissions factor can be calculated as:

$$EF_{CO}\left(\frac{g\,CO}{kg\ fuel}\right) = \frac{28 \cdot 860 \cdot \frac{CO}{CO_2}}{\left(1 + \frac{CO}{CO_2} + 6\frac{HC}{CO_2}\right) \cdot 12} = 2007\left(\frac{CO}{CO_2 + CO + 6HC}\right)$$

$$EF_{HC}\left(\frac{g\,HC}{kg\ fuel}\right) = \frac{2 \cdot 44 \cdot 860 \cdot \frac{HC}{CO_2}}{\left(1 + \frac{CO}{CO_2} + 6\frac{HC}{CO_2}\right) \cdot 12} = 6306\left(\frac{HC}{CO_2 + CO + 6HC}\right)$$

$$EF_{NO}\left(\frac{g\,NO}{kg\ fuel}\right) = \frac{30 \cdot 860 \cdot \frac{NO}{CO_2}}{\left(1 + \frac{CO}{CO_2} + 6\frac{HC}{CO_2}\right) \cdot 12} = 2150\left(\frac{NO}{CO_2 + CO + 6HC}\right)$$

$$EF_{PM}\left(\frac{g\,PM}{kg\,fuel}\right)=\frac{\left(\frac{1g}{1000\,mg}\right)\left(860\frac{g\,C}{kg\,fuel}\right)\cdot PM}{\left(CO_2+CO+6HC\right)\left(12\frac{g\,C}{mole}\right)\left(41\frac{mole}{m^3}\right)}$$

$$=0.00175\left(\frac{PM\left(\frac{mg}{m^3}\right)}{CO_2+CO+6HC}\right)$$

Where the gas concentrations CO_2, CO, HC, NO have units of atmospheres and PM has units of mg/m3. The fuel based emissions factors were calculated for PM only if valid measurements were available for CO_2. If CO and HC were also valid, their concentrations were also included in the emissions factor calculation.

4.2 Measurement Results

The results of the remote sensing parking lot tests conducted on 2001/02/21 are summarized in Table 1. Each vehicle was driven through the remote sensing test section 5 times for a specified speed (i.e., 10 mph, 20 mph, and 30 mph). The table shows the average of all valid emissions factors for each vehicle operating at each speed. The standard deviation and number of replicate measurements are also shown for each vehicle/speed combination.

The default data validation criteria for the RSD3000 requires that the CO_2 extinction measured in the exhaust plume be larger than a specified limit. On multiple passes, this criteria was not met and emissions factors could not be calculated for CO, NO, HC, and PM. Data recovery rates for the entire set of tests ranged from 57% for NO to 65% for CO and PM.

The standard deviation of the PM emissions factors for the Club Wagon and the Isuzu were quite large (6.8 g/kg fuel and 8.5 g/kg fuel) with respect to those measured on the F250 (1.0 – 1.1 g/kg fuel). The source of this discrepancy is unknown at this time, but may be related to the location of the exhaust pipe within the LIDAR field of view.

Table 1 also shows the average of the observed vehicle speed and acceleration as measured by the speed and acceleration strips. For most parking lot tests, the absolute value of average acceleration was less than 1 kph/s. The one exception to this was the 10 mph runs with the Isuzu. Variations in the vehicle acceleration are likely to influence the PM emissions factors since the operating mode of the engine is most sensitive to acceleration.

Table 2 shows the summary of the emissions factors from the same vehicles measured on the freeway onramp on 2001/02/22. Data recovery rates for these tests were similar to those of the previous day: 54% for NO and 62% for CO and PM. With the exception of the Isuzu vehicle, the standard deviations of the PM measurements were all less than 1.1 g/kg fuel for all tests from each vehicle. Three of the four valid PM measurements from the Isuzu (corresponding to the 30 mph tests) had an average acceleration of 1.3 kph/s while the accelerations from the other vehicles were less than 1.0 kph/s.

On both days, average measured PM emissions factors from the F250 were higher for the first set of measurements when compared with the second set of measurements. Relative differences

were 10% in the parking lot tests and 40% on the freeway onramp. These differences are substantially less than the variation of replicate measurements for either set of test series.

Table 1. Results of Parking Lot Tests for Select Diesel Vehicles on 2001/02/21.

Vehicle	Target Speed	Obs. Speed (kph)	Accel (kph/s)	EF CO (g/kg fuel)	EF CO (Std)	EF CO (n)	EF HC (g/kg fuel)	EF HC (Std)	EF HC (n)	EF NO (g/kg fuel)	EF NO (Std)	EF NO (n)	EF PM (g/kg fuel)	EF PM (Std)	EF PM (n)
Club Wagon	10 mph	17	-0.3	5.3	8.3	4	4.2	5.0	5	23.6	2.4	5	-0.1	7.6	4
	20 mph	31	-0.1	3.5	1.8	5	0.7	2.9	5	15.7	1.3	5	-3.0	6.0	5
	30 mph	44	0.6	5.9	2.2	5	2.5	3.2	4	13.7	2.4	4	-0.5	8.1	5
Club Wagon	**All**	**31**	**0.1**	**4.9**	**4.4**	**14**	**2.5**	**3.9**	**14**	**18.0**	**4.8**	**14**	**-1.3**	**6.8**	**14**
Ford F250 (Series1)	10 mph	15	0.0	8.4	6.0	3	6.7	2.6	3	28.3	1.0	2	0.2	1.9	3
	20 mph	31	-0.1	8.3	5.5	4	3.2	0.4	4	19.4	2.5	4	1.5	0.6	4
	30 mph	48	0.5	5.3	2.9	4	3.2	0.8	5	24.4	4.7	5	1.5	0.7	5
Ford F250 (Series1)	**All**	**32**	**0.1**	**7.3**	**4.6**	**11**	**4.1**	**2.0**	**12**	**23.3**	**4.8**	**11**	**1.2**	**1.1**	**12**
Ford F250 (Series2)	10 mph	15	0.1	14.6	11.9	3	2.2	2.1	3	16.5	1.6	3	0.8	0.8	3
	20 mph	34	-0.1	12.6	0.9	2	3.3	0.5	2	16.9	0.8	2	0.5	0.7	2
	30 mph	47	0.2	12.6	5.8	4	4.0	0.6	4	19.6	6.4	4	1.6	1.3	4
Ford F250 (Series2)	**All**	**31**	**0.1**	**13.3**	**7.0**	**9**	**3.2**	**1.4**	**9**	**18.0**	**4.3**	**9**	**1.1**	**1.0**	**9**
Isuzu	10 mph	16	3.1	4.9	11.2	3	1.2	6.4	3			0	-0.9	8.5	3
	20 mph	34	-0.2			0			0			0			0
	30 mph	45	0.2	4.0	N/A	1			0			0	8.8	N/A	1
Isuzu	**All**	**32**	**1.1**	**4.7**	**9.1**	**4**	**1.2**	**6.4**	**3**			**0**	**1.5**	**8.5**	**4**
All Vehicles		**31**	**0.4**	**7.5**	**6.5**	**38**	**3.1**	**3.1**	**38**	**19.7**	**5.2**	**34**	**0.3**	**4.9**	**39**

Table 2. Results of Freeway Onramp Tests for Select Diesel Vehicles on 2001/02/22.

Vehicle	Target Speed	Obs. Speed (kph)	Accel (kph/s)	EF CO (g/kg fuel)	EF CO (Std)	EF CO (n)	EF HC (g/kg fuel)	EF HC (Std)	EF HC (n)	EF NO (g/kg fuel)	EF NO (Std)	EF NO (n)	EF PM (g/kg fuel)	EF PM (Std)	EF PM (n)
Club Wagon	20 mph	35	0.6	-0.5	4.2	5	1.5	1.2	4	12.2	1.4	4	1.5	1.3	5
	30 mph	47	1.0	0.7	8.7	4	1.1	1.6	4	14.0	1.9	3	1.3	0.9	4
Club Wagon	**All**	**41**	**0.8**	**0.0**	**6.1**	**9**	**1.3**	**1.3**	**8**	**12.9**	**1.8**	**7**	**1.4**	**1.1**	**9**
Ford F250 (Series 1)	20 mph	34	0.0	18.3	15.9	5	3.2	2.3	5	17.3	2.5	5	1.3	0.5	5
	30 mph	47	0.5	7.0	0.7	4	2.5	1.4	4	19.0	5.7	4	1.5	0.3	4
Ford F250 (Series 1)	**All**	**40**	**0.2**	**13.3**	**12.7**	**9**	**2.9**	**1.9**	**9**	**18.0**	**4.0**	**9**	**1.4**	**0.4**	**9**
Ford F250 (Series 2)	20 mph	33	-0.1	8.3	4.8	4	2.9	3.0	4	19.9	2.1	3	1.0	1.3	4
	30 mph	51	0.8	12.0	14.3	4	1.7	1.8	5	28.0	4.9	5	1.0	0.8	5
	Hard Accel	27	10.3			0			0			0			0
Ford F250 (Series 2)	**All**	**36**	**4.1**	**10.1**	**10.0**	**8**	**2.3**	**2.3**	**9**	**25.0**	**5.7**	**8**	**1.0**	**1.0**	**9**
Isuzu	20 mph	39	0.6	-10.7	N/A	1	0.3	N/A	1	6.2	N/A	1	5.9	N/A	1
	30 mph	50	1.3	38.4	13.6	3	2.2	N/A	1	5.3	N/A	1	15.6	3.5	3
	Hard Accel	36	1.9			0			0			0			0
Isuzu	**All**	**41**	**1.4**	**26.1**	**26.9**	**4**	**1.2**	**1.3**	**2**	**5.8**	**0.6**	**2**	**13.1**	**5.6**	**4**
All Vehicles		**39**	**1.9**	**10.2**	**15.0**	**30**	**2.1**	**1.9**	**28**	**17.9**	**7.1**	**26**	**2.8**	**4.5**	**31**

5. REFERENCES

Barber, P.W. and S.C. Hill (1990). *Light Scattering by Particles – Computational Methods*, World Scientific, Singapore.

Bessagnet, B. and R. Roset (2001). Fractal modeling of carbonaceous aerosols – application to car exhaust plumes. Atmospheric Environment 35, 4751-4762.

Bishop, G.A. (2002). Personal Communication.

Cadle, S.H., P Mulawa, J. Ball, C. Donase, A. Weibel, J.C. Sagebiel, K.T. Knapp, and R. Snow (1997). Particulate emission rates from in-use high-emitting vehicles recruited in Orange County, California. Environ. Sci. Technol., 31:3405-3412.

Hansen, A.D.A., and H. Rosen (1990). Individual measurements of the emission factor of aerosol black carbon in automobile plumes, J. Air Waste Manage. 40:1654-1657.

Horvath, H. (1993). Atmospheric light absorption – a review, Atmospheric Environment 27A, 293-317.

Kittelson, D.B. (1998). Engines and nanoparticles: a review, J. Aerosol Science 29, 575-588.

Lawson, D.R. and R.E. Smith (1998). The Northern Front Range Air Quality Study: A report to the Governor and General Assembly. Prepared for the NFRAQS Governing Board by Colorado State University, December 1998.

Martins, J., P. Artaxo, C. Liousse, J. Reid, P. Hobbs, and Y. Kaufman (1998). Effects of black carbon content, particle size, and mixing on light absorption by aerosols from biomass burning in Brazil. Journal of Geophysical Research 103, 32,041-32,050.

Measures, R.M. (1992), *Laser Remote Sensing*, Kreiger, Malabar, Florida, eq. (7.23).

Morris, J.A., G.A. Bishop, D.H. Stedman (1998). On-road remote sensing of heavy-duty diesel truck emissions in the Austin-San Marcos Area: August 1998. Prepared by University of Denver, Department of Chemistry and Biochemistry, Denver, CO 80208, for Espey, Huston & Associates, Inc., P.O. Box 519, Austin TX 78767.

Sagebiel, J.C., B. Zielinska, P.A. Walsh, J.C. Chow, S.H. Cadle, P. Mulawa, K.T. Knapp, R.B. Zweidinger and R. Snow (1997). PM-10 exhaust samples collected during IM-240 dynamometer tests of in-service vehicles in Nevada, Environ. Sci. Technol., 31:75-83.

Seinfeld, J. and S. Pandis (1998), *Atmospheric Chemistry and Physics*, Wiley-Interscience, New York, eq. (7.34), eq. (7.52).

Shi, J.P., D. Mark, and R.M. Harrison (2000). Characterization of particles from a current technology heavy-duty diesel engine, Environ. Sci. Technol. 34, 748-755.

Stedman, D.H. and G.A. Bishop (1990). An analysis of on-road remote sensing as a tool for automotive emissions control. Final report to the Illinois Department of Energy and Natural Resources. ILENR/RE-AQ-90/05.

Stedman, D.H. and G.A. Bishop (1996). Measuring the emissions of passing cars, Acc. Chem. Res. 29, 489-495.

Toon, O. and T. Ackermann (1981). Algorithms for the calculation of scattering by stratified spheres, Appl. Opt., 20, 3657-3660.

Völger, P., J. Bösenberg, and I. Schult (1996). Scattering properties of selected model aerosols calculated at UV-wavelengths: implications for DIAL measurements of tropospheric ozone, Beitr. Phys. Atmosph. 69, 177-187.

APPENDIX: CONVERSION OF EXHAUST CONTENT TO FUEL BASED EMISSIONS FACTOR

This derivation was prepared by Gary Bishop of the University of Denver in 2002.

FEAT Equations for CO, HC and NO.

ASSUMPTIONS:

Fuel C:H ratio is 2 and non-oxygenated.
Fuel density is 0.726 g/ml and is approximated with a mix of Octane and Benzene that averages the molecular formula of CH_2.
Fuel out tailpipe is similar (to make the math simpler we have chosen for the exhaust HC to be a multiple of the input HC) to calibration gas which is propane.
Concentrations are calculated on a dry basis and corrected for any excess air not involved in combustion (these equations are correct for diesel vehicles, and the ratios are correct for diesel vehicles. However, if remote sensing data are to be compared to a direct tailpipe measurement, that measurement comparison either must consider only the ratios, or must be corrected for the considerable excess oxygen not involved in typical diesel combustion).
Equal amount of seen HC's and unseen HC's in the exhaust (Singer & Harley et al, Environ. Sci Technol. 1998, 32, 3241-3248)

$$CH_2 + m(0.21O_2 + 0.79N_2) \rightarrow aCO + bH_2O + c(C_3H_6 + inv\ C_3H_6) + dCO_2 + eNO + (0.79m - \frac{e}{2})N_2$$

$$Q = \frac{CO}{CO_2} = \frac{a}{d} \qquad Q' = \frac{HC}{CO_2} = \frac{c}{d} \qquad Q'' = \frac{NO}{CO_2} = \frac{e}{d}$$

by Carbon balance : a + 6c + d = 1

by Hydrogen balance: 2b + 12c = 2

by Oxygen balance: a + b + 2d + e= 0.42m

Eliminate a: a = dQ and c = dQ'

a + 6c + d = 1; dQ + 6dQ' + d = 1

$$d = \frac{1}{Q + 6Q' + 1}$$

Eliminate b: 2b + 12dQ' = 2 ; b = 1 - 6dQ'

dQ + b + 2d + e= 0.42m; dQ + 1 - 6dQ' +2d + e= 0.42m

substituting d from above:

$$0.42\ \frac{m}{d} = Q + \frac{1}{d} - 6Q' + 2 + Q'' = Q + Q + 6Q' + 1 - 6Q' + 2 + Q'' = 2Q + 3 + Q''$$

From the combustion equation the mole fraction of CO_2 is:

$$fCO_2 = \frac{d}{a + 2c + d + e + 0.79m - \frac{e}{2}}$$

divide numerator and denominator by d:

$$fCO_2 = \frac{1}{\frac{a}{d} + 2\frac{c}{d} + 1 + 0.5\frac{e}{d} + 0.79\frac{m}{d}}$$

substituting from above for a/d, c/d and e/d to get:

$$fCO_2 = \frac{1}{Q + 2Q' + 1 + 0.5Q'' + 0.79\frac{m}{d}}$$

multiply numerator and denominator by 0.42:

$$fCO_2 = \frac{0.42}{0.42Q + 0.84Q' + 0.42 + 0.21Q'' + (0.79)(0.42\frac{m}{d})}$$

substituting from above (0.42 m/d = 2Q + 3 + Q") leads to:

$$fCO_2 = \frac{0.42}{2.79 + 2Q + 0.84Q' + Q''}$$

from which follows:

$$\%CO_2 = \frac{42}{2.79 + 2Q + 0.84Q' + Q''} = \frac{100}{6.64 + 4.76Q + 2Q' + 2.38Q''}$$

$$\%CO = Q * \%CO_2 \qquad \%HC = Q' * \%CO_2 \qquad \%NO = Q'' * \%CO_2$$

Some useful conversions are:

For grams/gallon assume fuel density of 726 g/l, a fuel carbon fraction of 86%, 3.79 l/gallon and for CO 28g/mole; for HC (propane, C_3H_8) 44g/mole for NO 30g/mole; for C 12g/mole:

$$\frac{gmCO}{gal} = \frac{28*Q*0.86*726*3.79}{(1+Q+6Q')*12}$$

$$\frac{gmHC}{gal} = \frac{2*44*Q'*0.86*726*3.79}{(1+Q+6Q')*12}$$

$$\frac{gmNO}{gal} = \frac{30*Q''*0.86*726*3.79}{(1+Q+6Q')*12}$$

We now prefer to use grams of pollutant/kg of fuel because it requires no assumption about the fuel density:

$$\frac{gmCO}{kg} = \frac{28*Q*860}{(1+Q+6Q')*12}$$

$$\frac{gmHC}{kg} = \frac{2*44*Q'*860}{(1+Q+6Q')*12}$$

$$\frac{gmNO}{kg} = \frac{30*Q''*860}{(1+Q+6Q')*12}$$

If you want to express the measured ratios in the units of other molecules, for example $gmNO_2/kg$ since all emitted NO will eventually oxidize in the atmosphere to NO_2, you only have to change the molecular weight of the species in the appropriate equation.